Biomedical Engineering Advances 2 (2021) 100007

Contents lists available at ScienceDirect

Biomedical Engineering Advances

journal homepage: www.elsevier.com/locate/bea

Modulation of stem cell response using biodegradable polyester films with different stiffness

Sofia Ribeiro[a,b], Eugenia Pugliese[b], Stefanie H. Korntner[b], Emanuel M. Fernandes[c,d], Manuela E. Gomes[c,d], Rui L. Reis[c,d], Yves Bayon[a], Dimitrios I. Zeugolis[b,e,f,*]

[a] Medtronic, Sofradim Production, Trevoux, France
[b] Regenerative, Modular & Developmental Engineering Laboratory (REMODEL) and Science Foundation Ireland (SFI) Centre for Research in Medical Devices (CÚRAM), National University of Ireland Galway (NUI Galway), Galway, Ireland
[c] B's Research Group, Research Institute on Biomaterials, Biodegradables and Biomimetics (I3Bs), University of Minho, Headquarters of the European Institute of Excellence on Tissue Engineering and Regenerative Medicine, AvePark, Parque de Ciência e Tecnologia, Zona Industrial da Gandra, 4805-017 Barco, Guimarães, Portugal
[d] ICVS/3B's – PT Government Associate Laboratory, Braga, Guimarães, Portugal
[e] Regenerative, Modular & Developmental Engineering Laboratory (REMODEL), Università della Svizzera Italiana (USI), Lugano, Switzerland
[f] Regenerative, Modular & Developmental Engineering Laboratory (REMODEL), Charles Institute of Dermatology, Conway Institute of Biomolecular and Biomedical Research and School of Mechanical and Materials Engineering, University College Dublin (UCD), Dublin, Ireland

ARTICLE INFO

Keywords:
Biodegradable polyesters
Substrate stiffness
Mechanotransduction
Stem cell fate

ABSTRACT

Matrix stiffness is a crucial regulator of cell fate in both *in vitro* and *in vivo* setting. Although studies with non-degradable polymers have contributed to our understanding of the influence of rigidity on cell response, very little work has been conducted with biodegradable polymers that constitute the building blocks of implantable devices. Herein, we investigated human bone marrow stem cell response as a function of rigidity (7 kPa, 10 kPa, 12 kPa, 22 kPa, 15 MPa elastic modulus values) that induced by five different aliphatic polyesters (tissue culture plastic with ~ 3 GPa rigidity was used as control). Cell morphology analysis revealed that stiff substrates stimulated a large cell area with defined stress fibres, whilst soft substrates prompted a small cell area without evident stress fibres. Immunocytochemistry analysis made apparent that YAP was accumulated at the nuclei when the cells were seeded on stiff substrates and at the cytoskeleton on soft substrates. Substrate stiffness did not affect ($p > 0.05$) the expression of positive (> 97% CD73, CD90, CD105, CD44), but increased ($p < 0.05$) the expression of negative (< 44% CD45, < 14% CD31, < 28% CD146) mesenchymal stem cell markers after 21 days of culture. With respect to trilineage differentiation, the 15 MPa substrate induced the highest ($p < 0.05$) calcium deposition and SPP1 mRNA expression in osteogenic media, the 22 kPa substrate induced the highest ($p < 0.05$) COMP and ACAN mRNA expression in chondrogenic media and the 10 kPa substrate induced the highest ($p < 0.05$) FABP4 and CEBPA mRNA expression in adipogenic media, all after 21 days in culture. Although some issues associated with degradation were encountered, our data clearly illustrate that biodegradable polymers also contribute to cell phenotype and function in a rigidity dependant manner.

1. Introduction

Cells sense matrix rigidity at molecular scale level via activation of mechanotransduction signalling pathways [e.g., focal adhesion kinase (FAK) and Rho-associated protein kinase (ROCK)] that control various cellular functions, including adhesion, migration, morphology, proliferation and differentiation [1–4]. For example, on stiff substrates (elastic modulus of 48–53 kPa at macro-level), cells exhibit a spread cellular morphology and large cell area with numerous FA complexes and robust actin stress fibres, whilst on soft substrates (elastic modulus of 13–16 kPa at macro-level), cells exhibit a circular and constrained morphology with immature FA complexes and disorganised actin filaments [5]. With respect to differentiation, several *in vitro* studies have demonstrated a substrate rigidity dependant osteogenic [6,7], chondrogenic [8], adipogenic [9,10], tenogenic [11], neural [12], mesodermal [13] and myogenic [14] commitment. Although these studies have provided important insights into the understanding of substrate stiffness on cell response, they are of little value to contemporary regenerative

* Corresponding author at: Regenerative, Modular & Developmental Engineering Laboratory (REMODEL) and Science Foundation Ireland (SFI) Centre for Research in Medical Devices (CÚRAM), National University of Ireland Galway (NUI Galway), Galway, Ireland.
E-mail address: dimitrios.zevgolis@ucd.ie (D.I. Zeugolis).

https://doi.org/10.1016/j.bea.2021.100007
Received 21 March 2021; Received in revised form 5 July 2021; Accepted 5 July 2021
Available online 7 July 2021

medicine, as they have used non-degradable materials, such as polyacrylamide and polydimethylsiloxane. To substantiate this, one should consider that tissue / implantable device mechanical properties mismatch is still associated with implant failure [15–18]. Thus, there is an urgent need to develop biodegradable polymer-based devices with tunable mechanical properties for efficient cell fate control.

Synthetic biodegradable polymers are extensively used in tissue engineering, regenerative medicine and drug delivery due to their acceptable cytocompatibility, tolerable biodegradability, tunable mechanical properties and readily processability into tissue-specific conformations in an affordable and scalable manner [19–24]. In particular, aliphatic polyesters [e.g. poly(ε-caprolactone) [25], poly(glycolic acid) [26], poly(lactic acid) [27], poly(dioxanone) [28], poly(trimethylene carbonate) [29]] and copolymers thereof are the raw materials of multiple regulatory body approved medical devices for a diverse range of clinical indications. Yet again, their capacity to control stem cell lineage commitment as function of monomer composition (and consequently rigidity) is still unclear.

Herein, five polyester films of different composition and consequently stiffness were fabricated using compression moulding and their influence on human stem cell adhesion and phenotype was investigated.

2. Materials and methods

2.1. Materials

The aliphatic polyesters used were poly(glycolide-co-caprolactone) composed by weight of 9.6% glycolide and 90.4% of caprolactone with elastic modulus of 7 ± 3 kPa (7 kPa PGCL 10/90); poly(glycolide-co-dioxanone-co-(trimethylene carbonate)) composed by weight of 56.8% glycolide, 15.5% dioxanone and 27.7% trimethylene carbonate with elastic modulus of 10 ± 3 kPa (10 kPa PGDTMC 55/15/30); poly(lactide-co-(trimethylene carbonate)) composed by weight of 79.1% lactide and 20.9% trimethylene carbonate monomer with elastic modulus of 12 ± 3 kPa (12 kPa PLTMC 80/20); poly(glycolide-co-lactide) composed by weight of 18.1% glycolide and 81.9% lactide with elastic modulus of 22 ± 9 kPa (22 kPa PGL 15/85); and poly(glycolide-co-lactide) composed by weight of 31.4% glycolide and 68.6% lactide with elastic modulus of 15,019 ± 2916 kPa (15 MPa PGL 30/70). All polymers used were biodegradable and produced by Medtronic (North Haven, USA). The elastic modulus values were determined in previous study of the group using atomic force microscopy (AFM) [30] (authors' note: as elastic modulus values can vary between tools and methods [31], in the Discussion section, we mention the method used to assess the mechanical properties of the various materials in the studies that we cite). Furthermore, the degradation properties of the materials in phosphate buffered saline at neutral pH for up to 21 days were assessed in previous study of our group [30] and the results are summarised in **Supplementary Table S1**. All tissue culture plastics were purchased from Sarstedt (Ireland). All chemicals, cell culture media and reagents were purchased from Sigma Aldrich (Ireland), unless otherwise stated.

2.2. Processing of polymeric films

The polymeric films were obtained by compression moulding, using a thermal presser Carver 3856 CE (Carver, USA), as has been described before [30]. In brief, the presser was heated close to the polymer melting temperature (7 kPa PGCL 10/90: 90 °C, 10 kPa PGDTMC 55/15/30: 220 °C, 12 kPa PLTMC 80/20: 220 ºC, 22 kPa PGL 15/85: 180 °C and 15 MPa PGL 30/70: 220 °C). The polymer pellets were placed between two metal sheets covered by Teflon sheets and subjected to a minimum pressure of 1 bar for 5 min. Subsequently, the system was gradually cooled down (10 °C/min) to approximately 30 °C. The fabrication method was performed under controlled temperature and humidity conditions. The settings were selected to obtain polymeric films of 200 μm in thickness. The produced films were stored in sealed aluminium bags in desiccants at 4 °C until use.

2.3. Human stem cell isolation and culture

Human bone marrow stem cells (hBMSCs) were isolated according to standard protocols [32]. Briefly, bone marrow obtained from the iliac crest was purchased from Caltag (UK). The bone marrow was washed in phosphate buffered saline (PBS) and subsequently plated on tissue culture plastic (3 GPa TCP) in α-minimal essential medium (αMEM) supplemented with 10% foetal bovine serum (FBS) and 1% penicillin streptomycin (P/S). Cells were cultured at 37 °C in a humidified atmosphere of 5% CO_2. After 7 days in culture, the non-adherent cells were removed by several washes with PBS and the adherent cells (passage 0) were cultured to 80% to 90% confluency. For passaging, cells were detached using trypsin-ethylenediaminetetraacetic acid (EDTA). Cells at passage 3 to 4 were used for all experiments. Prior to cell seeding, the polymeric films were sterilised with ethylene oxide at Medtronic (USA). hBMSCs at passage 3 to 4 were detached using trypsin-EDTA, washed with PBS and centrifuged at 800 g for 5 min. The cell pellet was resuspended in αMEM supplemented with 10% FBS and 1% P/S. Subsequently, 100 μl of the cell suspension were poured on top of the films, which were placed at the bottom of 24 well plates. The cells were allowed to attach for 2.5 h prior to adding 900 μl of complete basal medium. The media were changed every other day. Cells seeded on 3 GPa TCP served as control group.

2.4. Stem cell morphology, focal adhesion, YAP distribution and ROCK inhibition analyses

For assessing *in vitro* cell morphology, cells were seeded onto polymeric films, at a density of 500 cells/cm^2 and were cultured in αMEM supplemented with 10% FBS and 1% P/S. After 6 and 24 h, cells were fixed with 4% paraformaldehyde (PFA) for 2 h at 4 ºC, blocked with 3% bovine serum albumin (BSA) in PBS for 30 min at room temperature (RT) and permeabilised with 0.2% Triton X-100 for 5 min at RT. The samples were incubated with rhodamine labelled phalloidin (66 μM in PBS, 1:200, Invitrogen, Ireland) for 2 h at RT to stain cytoskeleton and with Hoechst 33,342 solution (20 mM in PBS, 1:5000, Invitrogen, Ireland) to stain nuclei for 5 min at RT. Fluorescent images were captured using an Olympus IX-81 inverted fluorescence microscope (Olympus Corporation, Japan) at 10x magnification. 3 replicates of each group were imaged and 5 field of view (FOV) were taken from each replicate (a total of 15 images were analysed per experimental group). Images were analysed with ImageJ (NIH, USA) for circularity and cell area. Circularity was assessed as a function of cell spreading, where circularity is 0 for elongated cells and 1 for a perfect circle. Cell area was assessed by quantification of rhodamine staining and normalised to cell number. Nuclei were counted to obtain cell number.

Focal adhesion kinase (FAK) gene expression was analysed after 6 h and 24 h of culture. Total RNA was isolated using the RNeasy Plus Micro Kit (Qiagen, Germany) according to the manufacturer's protocol. Briefly, samples were disrupted in Buffer RLT and homogenised. Ethanol was then added to the lysate and the samples were transferred to the RNeasy Micro spin column. All bind, wash and elution steps were performed by centrifugation in a microcentrifuge. Total RNA was retained in the membrane (bind step), contaminants were efficiently washed away (wash step) and high-quality RNA was eluted in RNase-free water (elution step). RNA concentration and purity were determined using a NanoDrop 1000 (Thermo Fisher Scientific, Ireland). Samples with RNA purity values of 260/280 ratio ~1.8 and 260/230 ratio ~1.9 were used for qPCR experiments. RNA integrity was assessed with an Agilent 2100 Bioanalyser (Agilent Technologies, Ireland). Samples with RNA integrity (RIN) values of > 8 were used for qPCR experiments. Samples with RIN < 8 were excluded from the study. 1 μg total RNA was reverse transcribed using the iScript^{TM} cDNA Synthesis Kit (Bio-Rad Laboratories, Ireland).

5 ng cDNA were subsequently analysed by qPCR on a StepOnePlus™ Real-Time PCR System (Thermo Fisher Scientific, Ireland), using TaqMan primer probe assays (IDT, Belgium) and TaqMan Gene Expression Mastermix (Thermo Fisher Scientific, Ireland). The TaqMan primer probe assays used are listed in **Supplementary Table S2**. The amplification conditions were 50 °C for 2 min, 95 °C for 10 min, followed by 40 cycles of 95 °C for 15 s and 60 °C for 1 min. qBasePlus v. 2.4 (Biogazelle NVBelgium) was used to perform geNorm analysis to determine the optimal number of reference genes. CQ values were analysed and normalised relative quantities (NRQs) were calculated by normalising the data to the expression of three validated endogenous control genes (EIF2B1, HPRT1, TBP) with qBasePlus v. 2.4 (Biogazelle, Belgium) [33].

For Yes-associated protein (YAP) analysis, samples were stained with a rabbit anti YAP antibody (10 mM in PBS, 1:200, D8H1Z, Cell Signalling Technology, USA) overnight at 4 °C. After 3 washes in PBS, samples were incubated for 2 h with a goat anti-rabbit Alexa Fluor 488® IgG antibody (2 mg/ml in PBS, 1:200, Invitrogen, Ireland) at RT. Subsequently, the samples were stained for rhodamine/Hoechst. Fluorescent images were captured using an Olympus IX-81 inverted fluorescence microscope (Olympus Corporation, Japan) at 10x magnification. For assessment of YAP expression and cell surface area and shape, cells were cultured on the various groups for 6 h. 3 replicates of each group were imaged and 5 field of view (FOV) were taken from each replicate (a total of 15 images were analysed per experimental group). YAP fluorescence was analysed in the nuclear region and the immediately adjacent cytoplasmic region by ImageJ software (NIH, USA). The corresponding Hoechst staining image was used to delimit nuclear versus cytoplasmic regions. The ratio was calculated by dividing each fluorescence value. For ROCK inhibition analysis, the hBMSC suspension was incubated for 3 h at 37 °C with ROCK inhibitor (*Y*-27,632 dihydrochloride) at a concentration of 10 μM in PBS before seeding. After 6 and 24 h, cells were fixed with 4% PFA for 2 h at 4 °C, blocked with 3% BSA in PBS for 30 min at RT and permeabilised with 0.2% Triton *X*-100 for 5 min at RT. Subsequently, the samples were stained for rhodamine/Hoechst. Fluorescent images were captured using an Olympus IX-81 inverted fluorescence microscope (Olympus Corporation, Japan) at 10x magnification. 3 replicates of each group were imaged and 5 field of view (FOV) were taken from each replicate (a total of 15 images were analysed per experimental group). Images were analysed with ImageJ (NIH, USA) for circularity and cell area. Circularity was assessed as a function of cell spreading, where circularity is 0 for elongated cells and 1 for a perfect circle. Cell area was assessed by quantification of rhodamine staining and normalised to cell number. Nuclei were counted to obtain cell number.

2.5. Flow cytometry analysis

Flow cytometry was conducted after 3 and 21 days in culture. Cells were incubated with various combinations of fluorochrome-labelled antibodies (**Supplementary Table S3**) to assess mesenchymal stem cell phenotype [stem cell positive (CD73, CD90, CD105, CD44) and negative (CD45, CD31, CD146) markers, along with their respective isotype controls] according to the manufacturer's instructions (BD Stemflow™, UK). In brief, cells were washed with cold PBS, trypsinised for 5 min and αMEM with 10% FBS was added to neutralise trypsin's activity. Cells were collected, washed with 2% FBS in PBS, centrifuged at 800 g for 5 min and the supernatant was removed. Cells were resuspended in 2% FBS in PBS and strained through a 40 μm cell strainer. Cells were counted and diluted to a concentration of 1 million cells per ml in 2% FBS in PBS. Subsequently, ~100,000 cells were placed in each tube and stained with the appropriate volume of fluorochrome-labelled antibodies for 30 min at RT. Cells were washed twice in PBS and resuspended in 2% FBS in PBS. Sytox blue (Invitrogen, Ireland) was used as viability dye. Cells were analysed using a fluorescence-activated cell sorting (FACS) equipment (BS FACSCanto™ II Cell Analyser, BD Biosciences, UK) and the percentage of positive cell populations were calculated using FlowJo® software v10 (TreeStar Inc., USA).

2.6. Stem cell DNA and metabolic activity analyses

DNA was quantified in basal and differentiation media using Quant-iT™ PicoGreen® dSDNA assay kit (Invitrogen, Ireland) according to the manufacturer's protocol. Briefly, after 14 and 21 days of culture, DNA was extracted using 3 freeze-thaw cycles after adding 250 μl of nucleic acid free water per well. 100 μl of sample were transferred into a 96-well plate. A standard curve was generated using 0, 5, 10, 25, 50, 100, 500 and 1000 ng/ml DNA concentrations. 100 μl in ultra-pure water of a 1:200 dilution of Quant-iT™ PicoGreen® reagent were added to each sample and the plate was read using a micro-plate reader (Varioskan Flash, Thermo Fisher Scientific, UK) with excitation wavelength of 480 nm and emission wavelength of 525 nm.

Metabolic activity was assessed in basal and differentiation media using the alamarBlue™ assay (Invitrogen, USA) according to the manufacturer's protocol. In brief, after 14 and 21 days of culture, cells were washed with Hanks' balanced salt solution (HBSS) and alamarBlue™ solution (10% alamarBlue™ in HBSS) was added. After 4 h of incubation at 37 °C, absorbance was measured in triplicate at excitation wavelength of 550 nm and emission wavelength of 595 nm using Varioskan Flash spectral scanning multimode reader (Thermo Fisher Scientific, UK). Cell metabolic activity was normalised to DNA content.

2.7. Osteogenic induction and differentiation analysis

Cells were seeded on the various substrates at density of 20,000 cells/cm^2. Cells were allowed to attach and spread for 48 h in αMEM supplemented with 10% FBS and 1% P/S (basal media). Osteogenesis was induced with 10 mM β-glycerophosphate disodium salt hydrate, 100 nM dexamethasone, 50 μM ascorbic acid-2-phosphate in αMEM supplemented with 10% FBS and 1% P/S. The differentiation media were changed every 3 days up to 21 days of incubation.

Osteogenic differentiation was assessed by quantification of calcium deposition using the StanBio Calcium Liquicolour™ Kit (Thermo Fisher Scientific, Ireland). Samples were digested with 0.5 M HCl overnight at 4 °C. A standard curve was generated using 0, 1, 5, 10, 30, 50 and 100 mg/ml calcium concentrations in 0.5 M HCl. 10 μl of cell lysate or standard and 200 μl of working solution were added to 96 well plate. The working solution was composed of 1 to 1 colour reagent to base reagent. absorbance at 550 nm was measured using a Varioskan Flash spectral scanning multimode reader (Thermo Fisher Scientific, UK) and the amount of calcium per well was calculated using calcium standards and normalised to the amount of DNA. Alkaline phosphatase (ALP) activity was assessed by lysing the cells with deionised water, frozen them at −80 °C and thawing them at RT (the freeze-thaw was done twice). 20 μl of the cell lysate and standard were incubated with 80 μl of 1-Step™ p-nitrophenyl phosphate (PNPP) Substrate Solution (Thermo Scientific, UK). After 30 min of incubation at 37 °C, the reaction was stopped by adding 100 μl of 0.05 M NaOH. Absorbance was measured at 405 nm using a Varioskan Flash spectral scanning multimode reader (Thermo Fisher Scientific, UK). The amount of p-nitrophenol was calculated using p-nitrophenol (10 mM 4-nitrophenol) standards and the units of the enzyme were calculated by dividing the μmoles of p-nitrophenol produced by time (min) and then by normalising them to the amount of DNA. Runt-related transcription factor 2 (RUNX2), osteopontin (SPP1), type I collagen (COL1A1) and bone sialoprotein (BSP) gene expression in basal and osteogenic media was analysed after 14 and 21 days (primer and probe sequences are provided in **Supplementary Table S2**).

2.8. Chondrogenic induction and differentiation analysis

Cells were seeded on the various substrates at density of 20,000 cells/cm^2. Cells were allowed to attach and spread for 48 h in αMEM

supplemented with 10% FBS and 1% P/S (basal media). Chondrogenesis was induced with 100 nM dexamethasone, 100X ITS+1 (insulin, transferrin, sodium selenite, linoleic-BSA) liquid media supplement, 40 μg/ml *L*-proline, 50 μg/ml ascorbic acid-2-phosphate, 10 ng/ml TGF-β3 in high glucose Dulbecco's Modified Eagle Medium (DMEM) supplemented with 1% P/S. The differentiation media were changed every 3 days up to 21 days of incubation. Metabolic activity was assessed after 14 and 21 days of culture in basal and differentiation media and normalised by DNA content.

Chondrogenic differentiation was analysed by quantifying sulphated glycosaminoglycan (GAG) deposition using the 1,9-dimethylmethylene blue (DMMB) method (Blyscan Sulfated Glycosaminoglycan Assay, Biocolor, UK) after 21 days of culture. Briefly, samples were digested in a solution of 50 μg/ml proteinase K in 100 mM K_2HPO_4 (pH 8.0) overnight at 56 ºC. Subsequently, proteinase K was inactivated by heating the sample for 10 min at 90 °C [34]. The cell lysates were centrifuged and the supernatant was collected. A standard curve was generated using bovine tracheal chondroitin 4-sulfate standard. 50 μl of cell lysate was transferred to a clean Eppendorf tube and 1 ml of dye reagent was added. After agitation, the samples were centrifuged and the supernatant was discarded without disrupting the pellet. 500 μl of dye dissociator were added to the samples and mixed. Absorbance was measured at 656 nm using a Varioskan Flash spectral scanning multimode reader (Thermo Fisher Scientific, UK). The GAG content of the pellets was normalised to the amount of DNA. SRY-Box Transcription Factor 9 (SOX9), cartilage oligomeric matrix protein (COMP), aggrecan (ACAN) and type II collagen (COL2A1) gene expression was analysed in basal and chondrogenic media after 21 days (primer and probe sequences are provided in **Supplementary Table S2**). GAG quantification and gene expression was only analysed after 21 days of culture in chondrogenic media to allow the formation of a cell cluster on top of the substrates, as previously described [35].

2.9. Adipogenic indication and differentiation analysis

Cells were seeded on the various substrates at density of 20,000 cells/cm^2. Cells were allowed to attach and spread for 48 h in αMEM supplemented with 10% FBS and 1% P/S (basal media). Adipogenesis was induced with 1 μM dexamethasone, 1 μM rosiglitazone, 0.5 mM 3-isobutyl-1-methyl-xanthine and 10 μg/ml insulin in high glucose DMEM supplemented with 10% FBS and 1% P/S. After 3 days of adipogenic induction, media were switched to adipogenic maintenance media (10 μg/ml insulin in high glucose DMEM supplemented with 10% FBS and 1% P/S). The differentiation media were changed every 3 days up to 21 days of incubation. Metabolic activity was assessed after 14 and 21 days of culture in basal and differentiation media and normalised by DNA content.

Adipogenic differentiation was evaluated by Oil Red *O* staining. After 14 and 21 days of culture, the cells were fixed with 4% PFA for 20 min at 4 ºC. A 0.5% Oil red *O* stock solution was dissolved in denoised water and added to the samples for 20 min at RT. The samples were washed 3 times in PBS and imaged using a brightfield microscope (Leica Microsystems, Germany). 3 replicates of each group were imaged and 5 field of view (FOV) were taken from each replicate (a total of 15 images were analysed per experimental group). The area covered by lipid deposits was quantified by ImageJ (NIH, USA). CCAAT/enhancer-binding protein alpha (CEBPA), fatty acid-binding protein 4 (FABP4) and peroxisome proliferator-activated receptor gamma (PPARG) gene expression was analysed in basal and adipogenic media after 14 and 21 days (primer and probe sequences are provided in **Supplementary Table S2**).

2.10. Statistical analysis

Data are expressed as mean ± standard deviation. All experiments were conducted at least in three independent replicates. Statistical analysis was performed using GraphPad v6.01 (GraphPad Software Inc., USA). One- or two- way ANOVA was used for multiple comparisons and a Tukey *post hoc* test was used for pairwise comparisons after confirming that the samples followed a normal distribution (Kolmogorov-Smirnov test) and had equal variances (Bartlett's and Levene's test for homogeneity of variances). When either or both of these assumptions were violated, nonparametric tests were used for multiple (Kruskal-Wallis test) and pairwise (Mann-Whitney test) comparisons. Statistical significance was accepted at $p < 0.05$.

3. Results

3.1. Stem cell morphology, focal adhesion, YAP distribution and ROCK inhibition analyses

Qualitative immunocytochemistry analysis (**Fig. 1A**) revealed that after 6 h and 24 h, cells on the 7 kPa PGCL 10/90 and 10 kPa PGDTMC 55/15/30 substrates adopted an elongated morphology and cells on the 12 kPa PLTMC 80/20, 22 kPa PGL 15/85 and 15 MPa PGL 30/70 substrates and on the 3 GPa TCP exhibited a spread morphology. Quantitative circularity analysis (**Fig. 1B**) made apparent that after 6 h and 24 h, cells on the 7 kPa PGCL 10/90 and 10 kPa PGDTMC 55/15/30 substrates exhibited significantly ($p < 0.05$) lower circularity than cells on the 12 kPa PLTMC 80/20, 22 kPa PGL 15/85 and 15 MPa PGL 30/70 substrates and on the 3 GPa TCP (only after 6 h). Quantitative cell area analysis (**Fig. 1C**) revealed that after 6 h and 24 h, cells on the 3 GPa TCP had significantly ($p < 0.05$) larger area than cells on the polymeric substrates and within the polymeric substrates, after 6 h cells on the 7 kPa PGCL 10/90 had significantly ($p < 0.05$) smaller area than cells on the 22 kPa PGL 15/85 and 15 MPa PGL 30/70 substrates and after 24 h, the 15 MPa PGL 30/70 substrate induced significantly ($p < 0.05$) higher cell area than the other substrates. FAK gene expression analysis (**Fig. 1D**) demonstrated that after 6 h, cells on the 22 kPa PGL 15/85 substrate had the highest ($p < 0.05$) relative FAK gene expression and after 24 h, cells on the 22 kPa PGL 15/85 substrate had significantly ($p < 0.05$) higher relative FAK gene expression compared to 7 kPa PGCL 10/90 substrate and 3 GPa TCP. Immunocytochemistry (**Fig. 2A**) and complementary nuclear (**Fig. 2B**) and cytoplasmic (**Fig. 2C**) YAP quantification revealed that after 6 h, cells on the 10 kPa PGDTMC 55/15/30 substrate had the lowest ($p < 0.05$) nuclear YAP value, whilst the 7 kPa PGCL 10/90 substrate induced the highest ($p < 0.05$) cytoplasmic YAP value. Cells on the 7 kPa PGCL 10/90, 10 kPa PGDTMC 55/15/30 and 12 kPa PLTMC 80/20 substrates exhibited the lowest ($p < 0.05$) nuclear / cytoplasmic ratio (**Fig. 2D**). When cells were incubated with ROCK inhibitor, qualitative immunocytochemistry analysis (**Supplementary Fig. S1A**) after 6 h and 24 h revealed that all substrates induced similar cell morphology and the 3 GPa TCP induced the largest cell area. Quantitative circularity analysis (**Supplementary Fig. S1B**) after 6 h and 24 h revealed no significant ($p > 0.05$) differences amongst all groups. Quantitative cell area analysis (**Supplementary Fig. S1C**) showed that after 6 h and 24 h, cells on the 3 GPa TCP had the largest ($p < 0.05$) cell area and no significant ($p > 0.05$) differences in cell area were detected within the polymeric substrates. It is worth noting that no significant ($p > 0.05$) differences were observed between the groups in cell number after 6 h and the 12 kPa PLTMC 80/20 induced the highest ($p < 0.05$) cell number after 24 h (**Supplementary Fig. S2**).

3.2. Stem cell surface marker analysis

Flow cytometry analysis (**Supplementary Fig. 3**) revealed that the majority of the cells at passage 3 were positive for CD73 (89.7%), CD90 (99.9%), CD105 (96.2%) and CD44 (99.8%) and negative for CD45 (0.095%), CD31 (2.88%) and CD146 (6.31%). Most of the cells seeded on the various substrates and on TCP after 3 and 21 days (**Table 1**) were also positive for CD73, CD90, CD105 and CD44 (lowest value detected

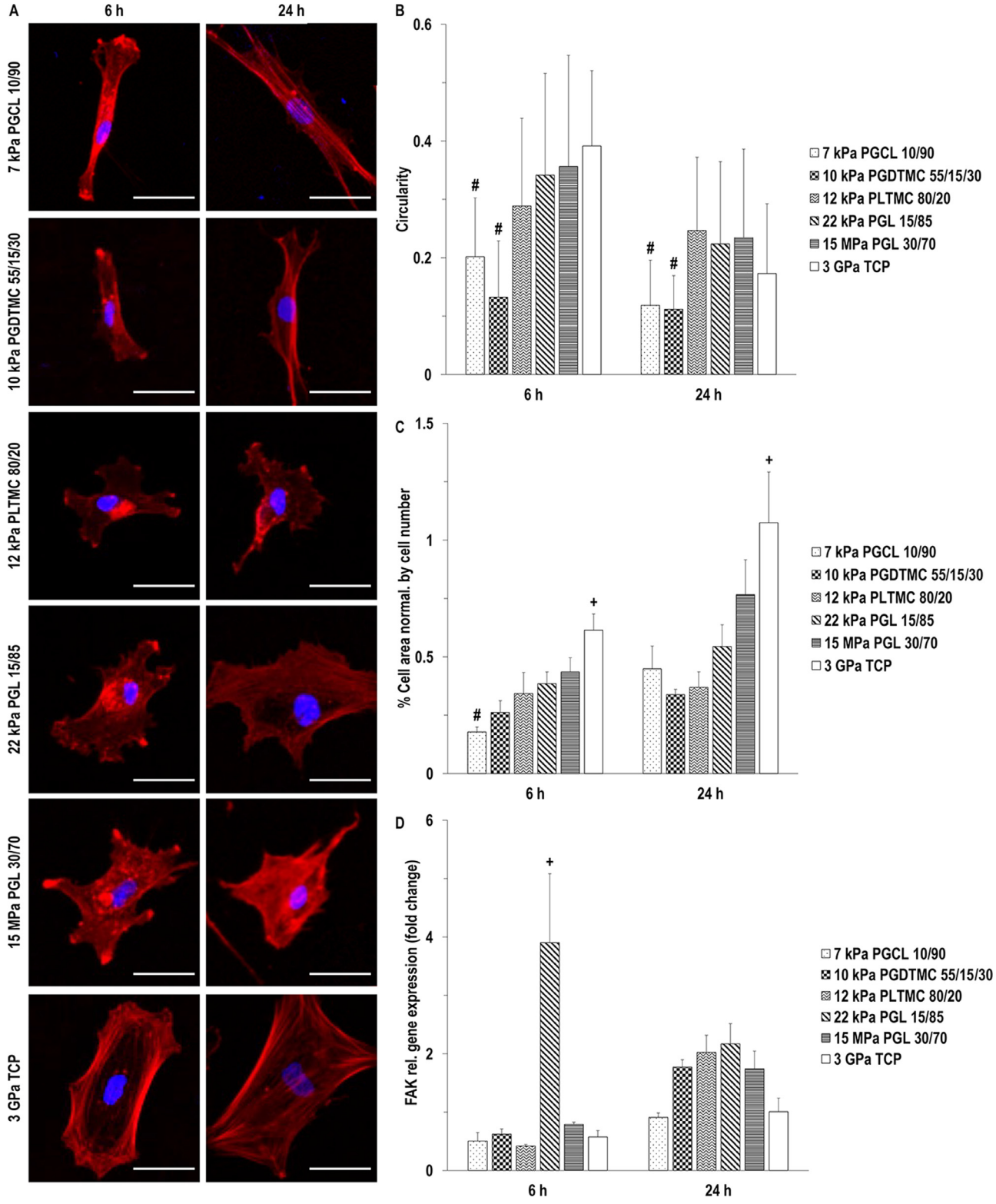

Fig. 1. Immunocytochemistry (A), circularity (B) and cell area (C) analyses revealed that the low in rigidity substrates induced low circularity and low cell area. The 22 kPa substrate exhibited the highest amongst all groups FAK mRNA expression after 6 h (D). Cytoskeleton: red. Nuclei: blue. Scale bars: 40 μm. # indicates lowest ($p < 0.05$) value at a given timepoint. + indicates highest ($p < 0.05$) value at a given timepoint. $N = 3$ (For interpretation of the references to color in this figure legend, the reader is referred to the web version of this article.).

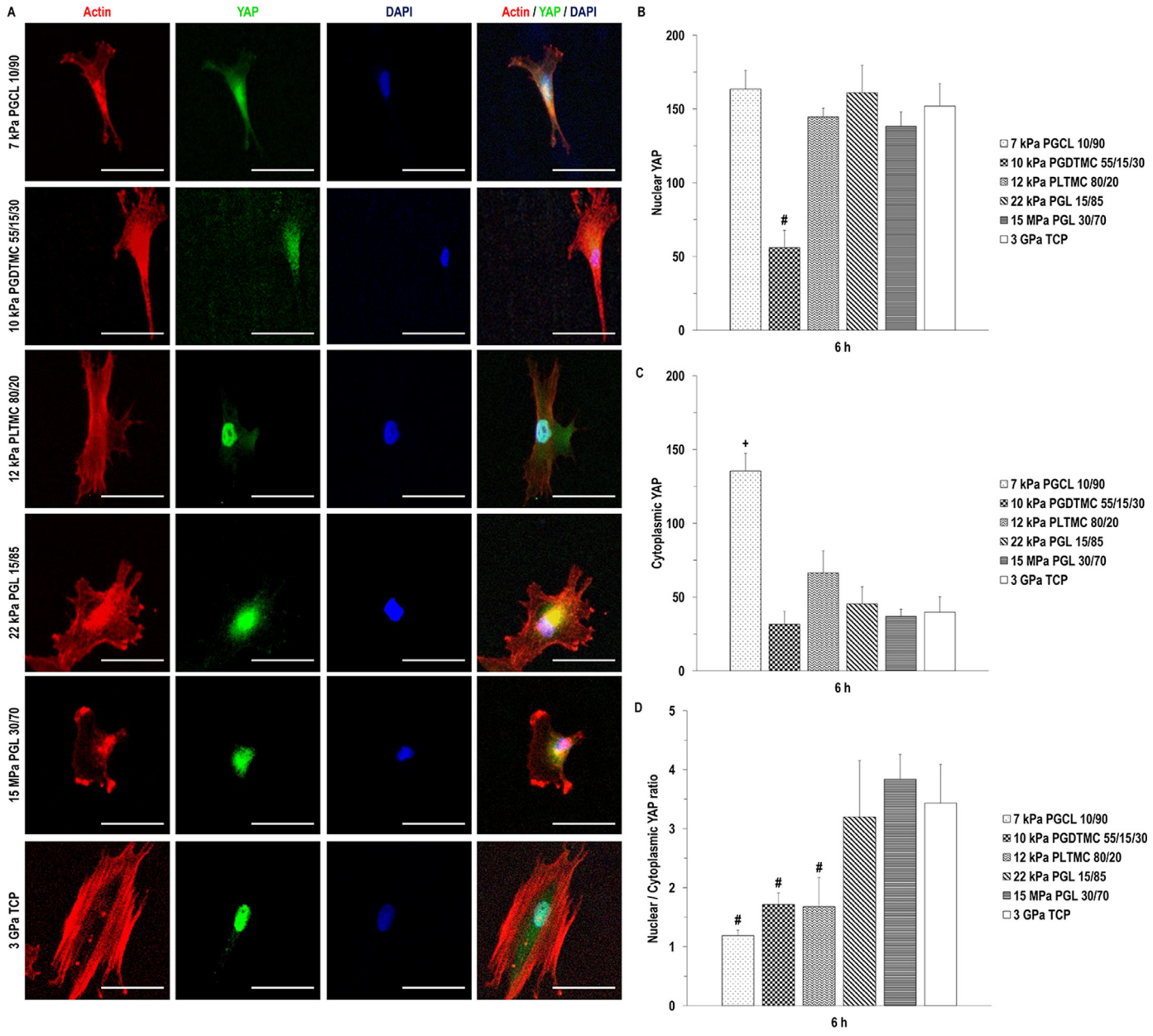

Fig. 2. Immunocytochemistry (A), nuclear YAP quantification (B), cytoplasmic YAP quantification (C) and nuclear / cytoplasmic ratio (D) analyses. Nuclear / cytoplasmic ratio analysis revealed that on the soft substrates, YAP was localised at the cytoskeleton, whilst on the stiff substrates, YAP was localised at the nuclei. YAP: green. Cytoskeleton: red. Nuclei: blue. Scale bars: 50 μm. # indicates lowest ($p < 0.05$) value at a given timepoint. + indicates highest ($p < 0.05$) value at a given timepoint. $N = 3$ (For interpretation of the references to color in this figure legend, the reader is referred to the web version of this article.).

was 88.4 ± 16.3% after 3 days for CD105 on cells seeded on the 12 kPa PLTMC 80/20). With respect to negative markers, at day 3, a small number of cells were positive for CD45 (lowest value of 2.2 ± 1.7% on 7 kPa PGCL 10/90 and highest value of 5.4 ± 2.7% on 10 kPa PGDTMC 55/15/30) and CD31 (lowest value of 0.9 ± 0.6% on 3 GPa TCP and highest value of 4.9 ± 1.0% on 10 kPa PGDTMC 55/15/30) and a relatively high number of cells were positive for CD146 (lowest value of 27.9 ± 0.2% on 15 MPa PGL 30/70 and highest value of 50.9 ± 2.1% on 7 kPa PGCL 10/90). At day 21, a relatively low number of cells were positive for CD31 (lowest value of 2.5 ± 0.7% on 10 kPa PGDTMC 55/15/30 and highest value of 13.8 ± 2.0% on 12 kPa PLTMC 80/20) and a relatively high numbers of cells were positive for CD45 (lowest value of 21.5 ± 5.7% on 10 kPa PGDTMC 55/15/30 and highest value of 43.1 ± 1.3% on 12 kPa PLTMC 80/20) and CD146 (lowest value of 19.5 ± 2.9 on% 22 kPa PGL 15/85 and highest value of 27.6 ± 21.2% on the 10 kPa PGDTMC 55/15/30).

3.4. Stem cell DNA and metabolic activity analyses

In basal media, at day 14, no significant ($p > 0.05$) differences were observed between the groups in DNA content and at day 21, the 3 GPa TCP induced the highest ($p < 0.05$) DNA content (**Supplementary Fig. S4A**). In osteogenic media, at day 14 (except from the 10 kPa PGDTMC 55/15/30 substrate) and day 21, the 15 MPa PGL 30/70 substrate induced the lowest ($p < 0.05$) DNA content (**Supplementary Fig. S4B**). In chondrogenic media, at day 14, the 12 kPa PLTMC 80/20 substrate induced the lowest ($p < 0.05$) DNA content and at day 14 and day 21, the 3 GPa TCP induced the high-

Table 1
After 3 and 21 days of culture, hBMSCs were evaluated for positive (CD73, CD90, CD105, CD44) and negative (CD45, CD31, CD146) mesenchymal stem cell markers. $N = 3$.

			7 kPa PGCL 10/90	10 kPa PGDTMC 55/15/30	12 kPa PLTMC 80/20	22 kPa PGL 15/85	15 MPa PGL 30/70	3 GPa TCP
Positive markers (% positive cells)	**CD73**	**3 days**	99.0 ± 0.1	99.9 ± 0.1	99.9 ± 0.1	99.9 ± 0.0	99.9 ± 0.1	99.0 ± 0.1
		21 days	99.9 ± 0.1	98.6 ± 0.2	99.8 ± 0.1	99.9 ± 0.0	99.9 ± 0.1	99.8 ± 0.2
	CD90	**3 days**	99.9 ± 0.0	99.9 ± 0.1	99.9 ± 0.1	99.9 ± 0.1	99.9 ± 0.0	99.9 ± 0.1
		21 days	99.9 ± 0.0	98.5 ± 0.2	99.7 ± 0.2	99.9 ± 0.1	99.9 ± 0.1	99.8 ± 0.0
	CD105	**3 days**	99.9 ± 0.2	94.6 ± 7.6	88.4 ± 16.3	99.5 ± 0.8	98.8 ± 1.8	99.6 ± 0.6
		21 days	99.9 ± 0.1	98.8 ± 0.1	99.9 ± 0.1	97.3 ± 3.7	99.9 ± 1.1	99.9 ± 0.1
	CD44	**3 days**	99.9 ± 0.1	99.8 ± 0.1	99.9 ± 0.1	99.8 ± 0.1	99.9 ± 0.1	99.9 ± 0.1
		21 days	99.9 ± 0.1	98.5 ± 0.3	99.8 ± 0.1	99.9 ± 0.1	99.8 ± 0.1	99.8 ± 0.1
Negative markers (% positive cells)	**CD45**	**3 days**	2.2 ± 1.7	5.4 ± 2.7	4.2 ± 2.7	2.8 ± 2.2	5.0 ± 3.6	3.4 ± 1.1
		21 days	36.5 ± 2.4	21.5 ± 5.7	43.1 ± 1.3	34.3 ± 1.3	27.1 ± 3.5	33.2 ± 2.3
	CD31	**3 days**	1.5 ± 0.3	4.9 ± 1.0	4.0 ± 1.0	2.0 ± 0.4	2.9 ± 0.7	0.9 ± 0.6
		21 days	7.8 ± 1.5	2.5 ± 0.7	13.8 ± 2.0	10.7 ± 1.5	6.2 ± 0.9	9.2 ± 1.5
	CD146	**3 days**	50.9 ± 2.1	32.0 ± 0.2	31.5 ± 0.2	44.2 ± 1.5	27.9 ± 0.2	38.5 ± 1.6
		21 days	21.2 ± 2.8	27.6 ± 21.2	22.6 ± 3.8	19.5 ± 2.9	24.8 ± 2.5	23.1 ± 2.3

est ($p < 0.05$) DNA content (**Supplementary Fig. S4C**). In adipogenic media, at day 14, the 7 kPa PGCL 10/90 substrate and the 3 GPa TCP induced the highest ($p < 0.05$) and the 22 kPa PGL 15/85 substrate induced the lowest ($p < 0.05$) DNA content and at day 21, the 7 kPa PGCL 10/90 substrate induced the highest ($p < 0.05$) DNA content (**Supplementary Fig. S4D**).

In basal media, at day 14 and day 21, the 15 MPa PGL 30/70 and the 22 kPa PGL 15/85 substrates induced the highest ($p < 0.05$) cell metabolic activity, respectively and, at both time points, the 7 kPa PGCL 10/90 and 10 kPa PGDTMC substrates and the 3 GPa TCP induced significantly ($p < 0.05$) lower cell metabolic activity than the other groups (**Supplementary Fig. S5A**). In osteogenic media, the 7 kPa PGCL 10/90 substrate induced the lowest ($p < 0.05$) cell metabolic activity at both timepoints and the 15 MPa PGL 30/70 induced the highest ($p < 0.05$) cell metabolic activity at day 21 (**Supplementary Fig. S5B**). In chondrogenic media, at day 14, the 12 kPa PLTMC 80/20 substrate induced the highest ($p < 0.05$) cell metabolic activity and the 7 kPa PGCL 10/90 induced the lowest ($p < 0.05$) cell metabolic activity and at day 21, the 3 GPa TCP induced the lowest ($p < 0.05$) cell metabolic activity (**Supplementary Fig. S5C**). In adipogenic media, at day 14 and day 21, the 22 kPa PGL 15/85 and the 15 MPa PGL 30/70 substrates induced significantly ($p < 0.05$) higher cell metabolic activity than the other groups and, at day 21, the 7 kPa PGCL 10/90 substrate induced the lowest ($p < 0.05$) cell metabolic activity amongst all groups (**Supplementary Fig. S5D**).

3.4. Osteogenic differentiation analysis

In basal media, all groups induced not detectable or very low calcium deposition at both timepoints (**Fig. 3A**); all groups induced below 20% alkaline phosphatase activity at both timepoints (**Fig. 3B**); the 7 kPa PGCL 10/90 and the 10 kPa PGDTMC 55/15/30 substrates induced the highest ($p < 0.05$) RUNX2 expression at day 21 (**Fig. 3C**); the 7 kPa PGCL 10/90 and the 10 kPa PGDTMC 55/15/30 substrates induced the highest ($p < 0.05$) SPP1 expression day 21 (**Fig. 3D**); the 7 kPa PGCL 10/90 and the 10 kPa PGDTMC 55/15/30 substrates induced the highest ($p < 0.05$) and the lowest ($p < 0.05$), respectively, COL1A1 expression at day 21 (**Fig. 3E**); the 7 kPa PGCL 10/90 and the 10 kPa PGDTMC 55/15/30 substrates induced the highest ($p < 0.05$) BSP expression at day 21 (**Fig. 3F**).

In osteogenic media, the 15 MPa PGL 30/70 [highest ($p < 0.05$) amongst all groups] and the 10 kPa PGDTMC 55/15/30 substrates induced the highest ($p < 0.05$) calcium deposition day 21 (**Fig. 3A**); the 12 kPa PLTMC 80/20 and the 22 kPa PGL 15/85 substrates induced the highest ($p < 0.05$) alkaline phosphatase activity at day 21 and 15 MPa PGL 30/70 substrates induced significantly ($p < 0.05$) lower alkaline phosphatase concentration compared to the 12 kPa PLTMC 80/20, the 22 kPa PGL 15/85 and the 3 GPa TCP at day 21 (**Fig. 3B**); the 3 GPa TCP and the 10 kPa PGDTMC 55/15/30 and the 12 kPa PLTMC 80/20 substrates induced the highest ($p < 0.05$) RUNX2 expression at day 21 and the 22 kPa PGL 15/85 induced the lowest ($p < 0.05$) RUNX2 expression at day 21 (**Fig. 3C**); the 15 MPa PGL 30/70 and the 7 kPa PGCL 10/90 substrates induced the highest ($p < 0.05$) and the lowest ($p < 0.05$), respectively, SPP1 expression at day 21 (**Fig. 3D**); the 3 GPa TCP and the 10 kPa PGDTMC 55/15/30 and 12 kPa PLTMC 80/20 substrates induced the highest ($p < 0.05$) COL1A1 expression at day 21 (**Fig. 3E**); the 10 kPa PGDTMC 55/15/30 and the 15 MPa PGL 30/70 substates and the 3 GPa TCP induced the highest ($p < 0.05$) BSP expression at day 21 (**Fig. 3F**).

3.5. Chondrogenic differentiation analysis

In basal media at day 21, all groups induced very low GAG synthesis (**Fig. 4A**); the 7 kPa PGCL 10/90 and the 10 kPa PGDTMC 55/15/30 substrates induced the highest ($p < 0.05$) SOX9 expression (**Fig. 4B**); the 10 kPa PGDTMC 55/15/30 substrate induced significantly ($p < 0.05$) higher COMP expression compared to 7 kPa PGCL 10/90, 22 kPa PGL 15/85 and 15 MPa PGL 30/70 substrate and 3 GPa TCP (**Fig. 4B**); and the 10 kPa PGDTMC 55/15/30 substrate induced the highest ($p < 0.05$) ACAN expression (**Fig. 4D**).

In chondrogenic media, the 10 kPa PGDTMC 55/15/30 substrate and the 3 GPa TCP induced the highest ($p < 0.05$) and the lowest ($p < 0.05$), respectively GAG synthesis (**Fig. 4A**); the 15 MPa PGL 30/70 substrate induced the highest ($p < 0.05$) SOX9 expression (**Fig. 4B**); the 22 kPa PGL 15/85 [highest ($p < 0.05$) amongst all groups] and the 15 MPa PGCL 30/70 substrates induced the highest ($p < 0.05$) COMP (**Fig. 4C**) and the 22 kPa PGL 15/85 substrate induced the highest ($p < 0.05$) ACAN (**Fig. 4D**) expression. No group induced COL2A1 expression neither in basal nor in chondrogenic media (data not shown).

3.6. Adipogenic differentiation analysis

In basal media, all groups induced not detectable or very low lipid droplet deposition (**Supplementary Fig. S6** and **Fig. 5A**), FABP4 expression (**Fig. 5B**) and PPARG expression (**Fig. 5C**) at both timepoints; and the 10 kPa PGDTMC 55/15/30 substrate induced the highest ($p < 0.05$) CEBPA expression at day 21 (**Fig. 5D**).

In adipogenic media, the 7 kPa PGCL 10/90 and the 10 kPa PGDTMC 55/15/30 substrates induced the highest ($p < 0.05$) lipid droplet deposition at day 21 (**Supplementary Figs. S6** and **Fig. 5A**); the 10 kPa PGDTMC 55/15/30 substrate induced the highest ($p < 0.05$) FABP4 expression at both timepoints (**Fig. 5B**); the 7 kPa PGCL 10/90 and the 15 MPa PGL 30/70 substrates induced the highest ($p < 0.05$) and the lowest ($p < 0.05$), respectively, PPARG expression at day 21 (**Fig. 5C**); the 10 kPa PGDTMC 55/15/30 substrate induced the highest ($p < 0.05$) CEBPA expression at day 21 (**Fig. 5D**).

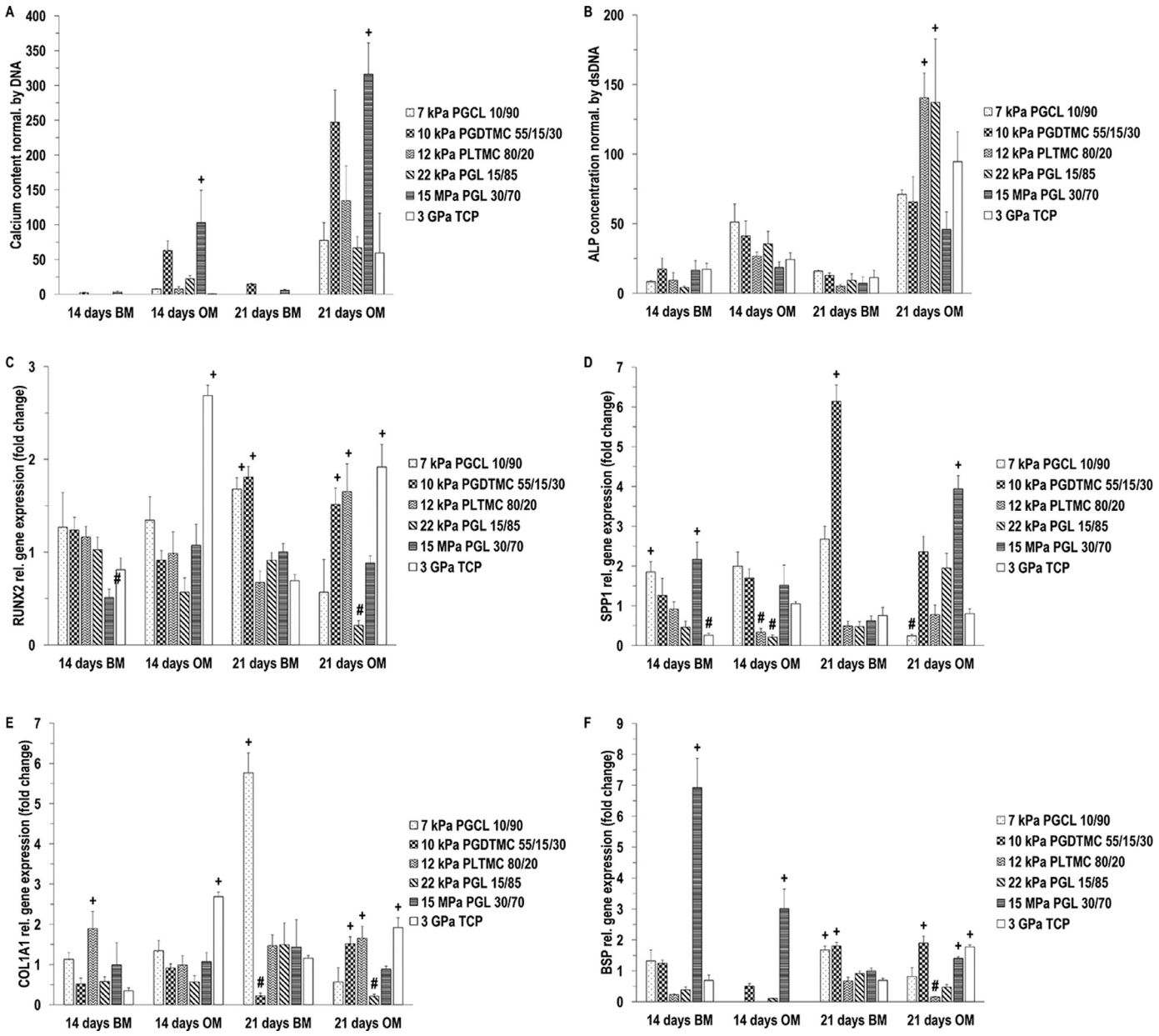

Fig. 3. In osteogenic media at day 21, the 15 MPa PGL 30/70 substrate induced the highest calcium deposition (A), the 12 kPa PLTMC 80/20 and the 22 kPa PGL 15/85 substrates induced the highest ALP deposition (B), the 10 kPa PGDTMC 55/15/30 and the 12 kPa PLTMC 80/20 substrates and the 3 GPa TCP induced the highest RUNX2 mRNA expression (C), the 15 MPa PGL 30/70 substrate induced the highest SPP1 mRNA expression (D), the 10 kPa PGDTMC 55/15/30 and the 12 kPa PLTMC 80/20 substrates and the 3 GPa TCP induced the highest COL1A1 mRNA expression (E) and the 10 kPa PGDTMC 55/15/30 and the 15 MPa PGL 30/70 substrates and the 3 GPa TCP induced the highest BSP mRNA expression (F). # indicates lowest ($p < 0.05$) value at a given timepoint. + indicates highest ($p < 0.05$) value at a given timepoint. $N = 4$.

4. Discussion

The influence of substrate rigidity is cell phenotype and function has been the subject of many investigations [36,37]. Although such work has provided significant insights on how cells respond to material-induced mechanotransduction signals, the vast majority of the work has been conducted with non-degradable polymers that are not customarily used in the development of implantable medical devices (**Supplementary Table S4**). Considering that numerous studies have reported clinical failure of implantable devices due to target tissue (and cell) mechanical properties mismatch, it is essential to assess the influence of substrate stiffness of biodegradable materials, that are the building blocks of most implantable devices, on cell fate. Herein, five polyester films with different elastic modulus (7 kPa PGCL 10/90, 10 kPa PGDTMC 55/15/30, 12 kPa PLTMC 80/20, 22 kPa PGL 15/85, 15 MPa PGL 30/70) were fabricated and their influence on hBMSC adhesion and phenotype was investigated. It is important to note that as the aim of the study was to assess the direct influence of these commercially available polymers that constitute the building blocks of many medical devices on stem cell behaviour, protein coating was not used and therefore mechanosensing occurred through local nascent protein deposition and remodelling [38].

Starting with cell morphometric analysis, in general, on stiff substrates (e.g., 22 kPa PGL 15/85 and 15 MPa PGL 30/70), the hBMSCs adopted a spread-out morphology, with big area and defined stress fibres, whilst on soft substrates (e.g., 7 kPa PGCL 10/90, 10 kPa PGDTMC

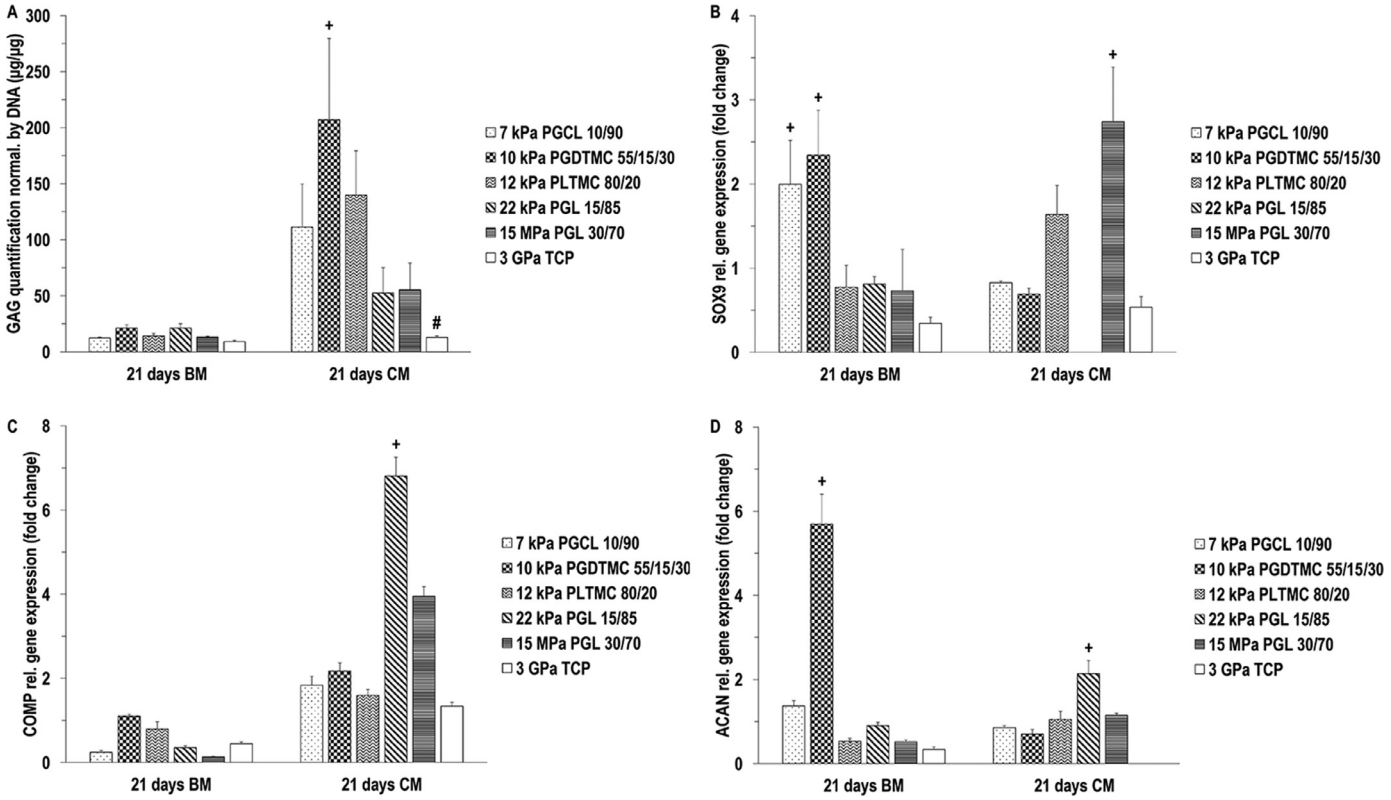

Fig. 4. In chondrogenic media at day 21, the 10 kPa PGDTMC 55/15/30 substrate induced the highest GAG deposition (A), the 15 MPa PGL 30/70 substrate induced the highest SOX9 mRNA expression (B), the 22 kPa PGL 15/85 substrate induced the highest COMP mRNA expression (C) and the 22 kPa PGL 15/85 substrate induced the highest ACAN mRNA expression (D). # indicates lowest ($p < 0.05$) value at a given timepoint. + indicates highest ($p < 0.05$) value at a given timepoint. $N = 4$.

55/15/30, 12 kPa PLTMC 80/20), the hBMSCs had small area and stress fibres were not evident. These observations are in accordance with numerous studies in the field, where, for example, it has been shown that hBMSCs on stiff PEG hydrogels (e.g. 36.8 kPa measured by AFM) exhibited a spread morphology with high spatial coverage, whilst on soft PEG hydrogels (e.g. 7.4 kPa measured by AFM), they showed reduced spreading [39].

Regarding the activation of mechanotransduction pathways, after 24 h, amongst the different polymeric films, the softest 7 kPa PGCL 10/90 film exhibited the lowest FAK gene expression, which is expected, considering that substrate stiffening leads to increased focal adhesion number and total FAK activation [40,41] and a linear correlation between focal adhesion size and cell spreading has been reported [42]. Of course, one would have expected the 3 GPa TCP to induce the highest FAK expression, which was not the case, possibly attributable to the short time period, considering that other studies assessed FAK expression after 3 [41] and 7 [40] days. Nonetheless, YAP analysis revealed that hBMSCs seeded on the stiffest conditions (e.g. 15 MPa PGL 30/70 substrate and 3 GPa TCP) showed the highest concentration of YAP in the nucleus, which further verifies previous studies demonstrating that stiff (elastic modulus of 25 kPa measured by AFM), as opposed to soft (elastic modulus of 2 kPa measured by AFM), collagen type I coated polyacrylamide hydrogels induced translocation of YAP to the nucleus [10,43,44]. Similarly, higher YAP activation was observed in hBMSCs seeded on poly(ethylene glycol) hydrogels in stiffer regions (~10 kPa measured by shear rheology) compared to softer (~2 kPa measured by shear rheology) regions [44]. It has been proposed that the strong mechanical feedback from stiff substrates leads to the unfolding of talins that expose binding domains for vinculins and activate YAP nucleus translocation to the cytoplasm [45,46]. Interestingly, the investigation of the inhibition of ROCK, a mechanotransducer that regulates both FAK and ERK1 [40], revealed that the data obtained were solely due to the elastic modulus of the substrates and not their chemical composition. Indeed, our results demonstrate that hBMSCs sense substrate stiffness via Rho-ROCK activated actomyosin contractility, as evidenced by the fact that stiffness-mediated changes in cell area and circularity were disappeared upon incubation with a ROCK inhibitor. These observations are in agreement with a previous published study, where ROCK inhibitor caused a reduction of cell spreading in fibroblasts cultured in 1, 6, and 20 kPa (measured by AFM) polyamide gels functionalised with collagen type I [47].

With respect to surface marker expression, our data showed that the expression of positive mesenchymal stem cell markers (CD73, CD90, CD105 and CD44) after 21 days of culture was not affected by the elastic modulus of the experimental groups, which is not in accordance with previous studies, where it was shown that culturing amniotic fluid-derived stem cells on 2 kPa and 5 kPa (mechanical properties characterisation method was not disclosed) collagen substrates resulted in increased cell surface marker expression of CD44, CD90 and CD105 compared to stiffer substrates (15 and 50 kPa, mechanical properties characterisation method was not disclosed), suggesting that the decrease in elastic modulus might mediate a recovery of some stem cell properties [48]. This disparity can be attributed to the lower rigidity, in comparison to ours, substrates that other studies have used (hBMSCs on 3.3 kPa poly(dimethylsiloxane) softer substrates exhibited higher percentage of CD44+ and CD73+ cells compared to stiffer 1.7 MPa and 1 GPa substrates measured by tensile testing [49]). The negative mesenchymal stem cell markers CD45 and CD31 were not affected by substrate stiffness or culture time and were within the range of expression previously published [50], suggesting that the cells maintained phenotype on the polymeric substrates and TCP. hBMSCs cultured in polymeric substrates and TCP showed increased expression of CD146, as has been shown

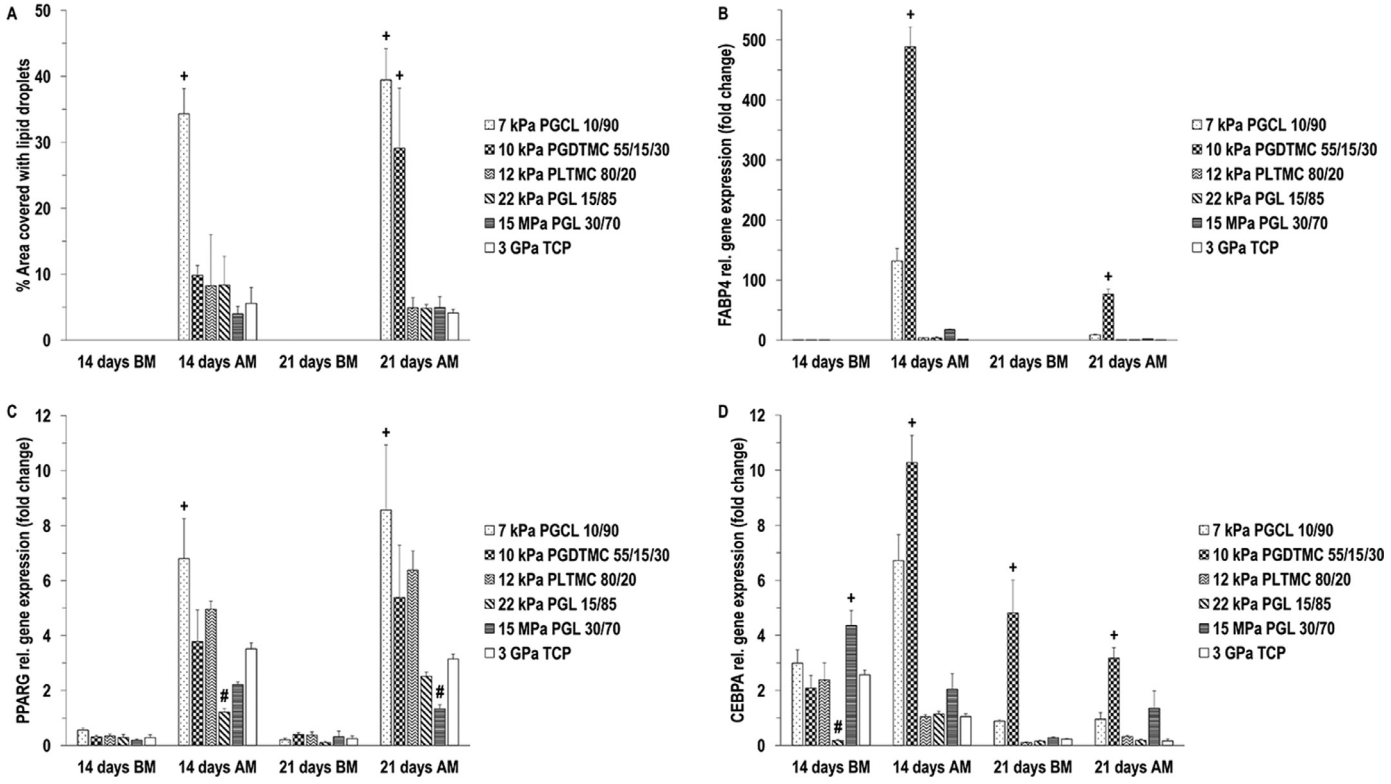

Fig. 5. In adipogenic media at day 21, the 7 kPa PGCL 10/90 and the 10 kPa PGDTMC 55/15/30 substrates induced the highest lipid droplets deposition (A), the 10 kPa PGDTMC 55/15/30 substrate induced the highest FABP4 mRNA expression (B), the 7 kPa PGCL 10/90 substrate induced the highest PPARG mRNA expression (C) and the 10 kPa PGDTMC 55/15/30 substrate induced the highest CEBPA mRNA expression (D). # indicates lowest ($p < 0.05$) value at a given timepoint. + indicates highest ($p < 0.05$) value at a given timepoint. $N = 4$.

before in Wharton's jelly derived stromal cell and hair follicle and spermatogonial stem cell cultures [50].

With respect to cell proliferation in basal media and DNA content and metabolic activity (normalised to DNA content) in basal and differentiation media, no clear trend was observed across all media and substrates, which may be attributed to the compositional differences of the media as opposed to the mechanical properties of the substrates. To substantiate this, one should note that all substrates induced almost similar proliferation in basal media at both timepoints (apart from the 12 kPa PLTMC 80/20 substrate) and the same substrates induced substantially different DNA content and metabolic activity at a given timepoint in different media. Nonetheless, in osteogenic and adipogenic media, the most rigid polymeric films (22 kPa PGL 15/85 and/or 15 MPa PGL 30/70) induced the highest metabolic activity. This is consistent with other studies in the field, where a stiff (20 kPa measured by micro-indentation) polyacrylamide substrate induced an increase in metabolic activity compared to a soft (1 kPa measured by micro-indentation) polyacrylamide substrate [51]. Similarly proliferative markers were higher in cells cultured on stiffer (1500 kPa measured by tensile testing) poly(dimethylsiloxane) substrates compared with those on softer (10 kPa measured by tensile testing) poly(dimethylsiloxane) substrates [52]. In chondrogenic media, no differences were observed between the substrates at day 21, which may be attributed to cell cluster formation that masked the influence of substrate stiffness.

In osteogenic media at day 21, the 15 MPa PGL 15/85 improved calcium deposition. A previous publication showed an increased calcium deposition on stiff (62–68 kPa measured by compression testing) fibronectin coated polyacrylamide hydrogels compared to soft (13–16 kPa measured by compression testing) fibronectin coated polyacrylamide hydrogels [5]. Furthermore, the 15 MPa PGL 15/85 caused an enhanced expression of SPP1, a late-stage osteogenic marker [2,53], as it has been observed before for dental pulp stem cells cultured on rigid (135 kPa measured by tensile testing), as opposed to soft (1.4 kPa measured by tensile testing), poly(dimethylsiloxane) hydrogels [54]. However, the 15 MPa PGL 15/85 substrate did not increase ALP content and did not upregulate the expression of other osteogenic markers (i.e., RUNX2 and BSP), as one would have expected. On the other hand, the 12 kPa PLTMC 80/20 and/or the 22 kPa PGL 15/85 substrates exhibited an enhanced effect on calcium content deposition, ALP content and RUNX2, COL1A1 and BSP expression. We attribute this to the degradation profile of the assessed polymers. Indeed, in a previous study of our group, we showed that, in PBS at 37 °C, the 7 kPa PGCL 10/90, 12 kPa PLTMC 80/20 and 22 kPa PGL 15/85 substrates maintained their tensile properties for up to 21 days, whilst the 15 MPa PGL 30/70 substrate started losing its elastic modulus as early as day 7 (shortest timepoint assessed) [30]. The documented quick degradability and loss of its mechanical properties (and as a direct consequence, loss of it capacity to effectively induce osteogenesis) of the 15 MPa PGL 30/70 is attributed to its high glycolide content, which is highly susceptible to the action of water [49].

In chondrogenic media at day 21, the 22 kPa PGL 15/85 film induced the highest COMP and ACAN expression, whilst SOX9, COL2A1 were not detected and GAG deposition was lower than the 7 kPa PGCL 10/90, 10 kPa PGDTMC 55/15/30 and 12 kPa PLTMC 80/20 substrates, similar to 15 MPa PGL 15/85 substrate and higher than the 3 GPa TCP. Whilst COMP and ACAN are late stage chondrogenic markers [55], we believe that 21 days is too late to see an expression for SOX9 in the 22 kPa PGL 15/85 film, which is an early stage chondrogenic marker [56]. With respect to collagen type II, we feel that the short period of the study is responsible for not been detected in any of the groups, considering that high COL2A1 expression occurs at later stages of chondrogenic differentiation (e.g. 28 days [57–60], 42–56 days [61–64], 84 days [65]). Another reason could be that the cells herein were cultured

on two-dimensional substrates and has been well established in the literature that chondrogenic induction requires three-dimensional culture [66]. GAG deposition was enhanced on softer substrates, in accordance with previously published work, where chondrocytes cultured on soft (1 kPa gelatine measured by tensile testing), as opposed to stiff (40 kPa gelatine measured by tensile testing), scaffolds exhibited higher GAG deposition [67].

With respect to the adipogenic potential of the various films assessed herein, in general, low in elastic modulus substrates (e.g., 7 kPa PGCL 10/90 and 10 kPa PGDTMC 55/15/30) showed an enhanced lipid deposition and an upregulation of adipogenic lineage specific markers (e.g., CEBPA, FABP4 and PPARG), in comparison to high in elastic modulus substrates (e.g., 22 kPa PGL 15/85, 15 MPa PGL 15/85, 3 GPa TCP). These results further validate previous observations, where hBMSCs cultured on a soft polyacrylamide substrate (elastic modulus of 2 kPa measured by AFM) showed increased expression of CEBPA and PPARG versus cells cultured on stiff substrates (elastic modulus of 25 kPa) [10]. Similarly, a previous study using polyacrylamide substrates with stiffness of 2 kPa, 20 kPa and 40 kPa measured by AFM showed that human adipose stem cells cultured in 2 kPa substrates induced higher expression of CEBPA and PPARG markers compared to stiffer substrates [68]. We attribute the highest expression of CEBPA and FABP4 on the 7 kPa PGCL 10/90 substrate to its lower degradability, in comparison to the 10 kPa PGDTMC 55/15/30 substrate [30].

When designing implantable devices, it is imperative to closely match the mechanical properties of the implantable devices to the mechanical properties of the tissue, as device / tissue mechanical properties mismatch is associated with implant failure [15–18]. Similarly, in cell culture technologies space, to maximise cellular functionality and therapeutic potential, it is of paramount importance to develop materials that will match the mechanical properties either of the tissue from which the cells were extracted from or of the tissue that will be implanted to. Although we recognise the simplicity in the use of TCP, we cannot but note that fails largely to imitate the mechanical properties of tissues (the elastic modulus of TCP is ~3 GPa [69], whilst the elastic modulus of pituitary gland is 3.5–25.9 kPa [70], buttock-thigh is 0.01 MPa [71], dermis is 0.10–0.25 MPa [72], tendon is 1 MPa [73], ligament is 1.1 MPa [74], articular cartilage is 2.6 MPa [75] and bone is 0.2–0.76 GPa [76]). This study further advocates the need to design bioinspired, with respect to mechanical properties, materials for both medical device and cell culture applications.

5. Conclusions

Although biodegradable polymers are the building blocks of most implantable medical devices, our knowledge on how substrate stiffness affects cell response has derived from studies utilising non-degradable polymers. In this study, the influence of five aliphatic polyesters of different elastic modulus (7 kPa, 10 kPa, 12 kPa, 22 kPa, 15 MPa) on human bone marrow stem cell fate and function was assessed. Our data clearly illustrate a biodegradable polymer rigidity-dependant cell response and advocate a more rational design in the engineering of implantable medical devices that, other than rigidity, will also take into consideration the degradation profile of the polymer.

Declaration of Competing Interest

SR was an early career researcher recruited at Sofradim Production, Medtronic, France and registered for PhD at NUI Galway, Ireland. YB is an employee of Sofradim Production, Medtronic, France. EP, SHK, EMF, MEG, RLR and DIZ declare no conflicts of interest.

CRediT authorship contribution statement

Sofia Ribeiro: Conceptualization, Writing – original draft, Data curation, Writing – review & editing, Formal analysis, Investigation, Methodology. **Eugenia Pugliese:** Formal analysis, Data curation, Investigation, Methodology, Writing – review & editing. **Stefanie H. Korntner:** Formal analysis, Data curation, Investigation, Methodology, Writing – review & editing. **Emanuel M. Fernandes:** Formal analysis, Data curation, Investigation, Methodology, Writing – review & editing. **Manuela E. Gomes:** Resources, Writing – review & editing. **Rui L. Reis:** Resources, Writing – review & editing. **Yves Bayon:** Resources, Writing – review & editing. **Dimitrios I. Zeugolis:** Supervision, Funding acquisition, Resources, Project administration, Conceptualization, Writing – original draft, Writing – review & editing.

Acknowledgments

This work has also received funding from the European Union's Horizon 2020 research and innovation programme under the Marie Skłodowska-Curie, grant agreement No. 676338, the European Research Council (ERC) under the European Union's Horizon 2020 research and innovation programme, grant agreement No. 866126 and the European Union's Horizon 2020 research and innovation Widespread: Twinning programme, grant agreement No. 810850. This publication has emanated from research supported in part by Grants from Science Foundation Ireland (SFI) under grant numbers 15/CDA/3629 and 19/FFP/6982 and Science Foundation Ireland (SFI) and European Regional Development Fund (ERDF) under grant number 13/RC/2073_2. This work was also supported by TERM RES Hub, Infraestrutura Científica para a Engenharia de Tecidos e Medicina Regenerativa, under grant number Norte-01-0145-FEDER-02219015.

Supplementary materials

Supplementary material associated with this article can be found, in the online version, at doi:10.1016/j.bea.2021.100007.

References

[1] G. De Santis, A.B. Lennon, F. Boschetti, B. Verhegghe, P. Verdonck, P.J. Prendergast, How can cells sense the elasticity of a substrate? An analysis using a cell tensegrity model, Eur. Cell Mater. 22 (2011) 202–213, doi:10.22203/ecm.v022a16.
[2] A. Higuchi, Q.D. Ling, Y. Chang, S.T. Hsu, A. Umezawa, Physical cues of biomaterials guide stem cell differentiation fate, Chem. Rev. 113 (2013) 3297–3328, doi:10.1021/cr300426x.
[3] A.J. Engler, S. Sen, H.L. Sweeney, D.E. Discher, Matrix elasticity directs stem cell lineage specification, Cell 126 (2006) 677–689, doi:10.1016/j.cell.2006.06.044.
[4] Y.S. Pek, A.C. Wan, J.Y. Ying, The effect of matrix stiffness on mesenchymal stem cell differentiation in a 3D thixotropic gel, Biomaterials 31 (2010) 385–391, doi:10.1016/j.biomaterials.2009.09.057.
[5] M. Sun, G. Chi, P. Li, S. Lv, J. Xu, Z. Xu, Y. Xia, Y. Tan, J. Xu, L. Li, Y. Li, Effects of matrix stiffness on the morphology, adhesion, proliferation and osteogenic differentiation of mesenchymal stem cells, Int. J. Med. Sci. 15 (2018) 257–268, doi:10.7150/ijms.21620.
[6] M. Sun, G. Chi, J. Xu, Y. Tan, J. Xu, S. Lv, Z. Xu, Y. Xia, L. Li, Y. Li, Extracellular matrix stiffness controls osteogenic differentiation of mesenchymal stem cells mediated by integrin alpha5, Stem Cell Res. Ther. 9 (2018) 52–65, doi:10.1186/s13287-018-0798-0.
[7] P.Y. Wang, W.B. Tsai, N.H. Voelcker, Screening of rat mesenchymal stem cell behaviour on polydimethylsiloxane stiffness gradients, Acta Biomater. 8 (2012) 519–530, doi:10.1016/j.actbio.2011.09.030.
[8] R. Olivares-Navarrete, E.M. Lee, K. Smith, S.L. Hyzy, M. Doroudi, J.K. Williams, K. Gall, B.D. Boyan, Z. Schwartz, Substrate stiffness controls osteoblastic and chondrocytic differentiation of mesenchymal stem cells without exogenous stimuli, PLoS ONE 12 (2017) e0170312–e0170330, doi:10.1371/journal.pone.0170312.
[9] T. Zhang, S. Lin, X. Shao, S. Shi, Q. Zhang, C. Xue, Y. Lin, B. Zhu, X. Cai, Regulating osteogenesis and adipogenesis in adipose-derived stem cells by controlling underlying substrate stiffness, J. Cell. Physiol. 233 (2018) 3418–3428, doi:10.1002/jcp.26193.
[10] A. Galarza Torre, J.E. Shaw, A. Wood, H.T.J. Gilbert, O. Dobre, P. Genever, K. Brennan, S.M. Richardson, J. Swift, An immortalised mesenchymal stem cell line maintains mechano-responsive behaviour and can be used as a reporter of substrate stiffness, Sci. Rep. 8 (2018) 8981–8993, doi:10.1038/s41598-018-27346-9.
[11] R.I. Sharma, J.G. Snedeker, Paracrine interactions between mesenchymal stem cells affect substrate driven differentiation toward tendon and bone phenotypes, PLoS ONE 7 (2012) e31504–e31514, doi:10.1371/journal.pone.0031504.g001.
[12] Y. Zhu, X. Li, R.R.R. Janairo, G. Kwong, A.D. Tsou, J.S. Chu, A. Wang, J. Yu, D. Wang, S. Li, Matrix stiffness modulates the differentiation of neural crest stem cells *in vivo*, J. Cell. Physiol. 234 (2019) 7569–7578, doi:10.1002/jcp.27518.

[13] N. Eroshenko, R. Ramachandran, V.K. Yadavalli, R.R. Rao, Effect of substrate stiffness on early human embryonic stem cell differentiation, J. Biol. Eng. 7 (2013) 7–14, doi:10.1186/1754-1611-7-7.
[14] K.W. Yong, Y. Li, F. Liu, G. Bin, T.J. Lu, W.A. Wan Abas, W.K. Wan Safwani, B. Pingguan-Murphy, Y. Ma, F. Xu, G. Huang, Paracrine effects of adipose-derived stem cells on matrix stiffness-induced cardiac myofibroblast differentiation via angiotensin II type 1 receptor and smad7, Sci. Rep. 6 (2016) 33067–33079, doi:10.1038/srep33067.
[15] M. Vatankhah-Varnosfaderani, W.F.M. Daniel, M.H. Everhart, A.A. Pandya, H. Liang, K. Matyjaszewski, A.V. Dobrynin, S.S. Sheiko, Mimicking biological stress-strain behaviour with synthetic elastomers, Nature 549 (2017) 497–501, doi:10.1038/nature23673.
[16] S. Prasadh, R.C.W. Wong, Unraveling the mechanical strength of biomaterials used as a bone scaffold in oral and maxillofacial defects, Oral Sci. Int. 15 (2018) 48–55, doi:10.1016/s1348-8643(18)30005-3.
[17] M. Gasik, A. Zuhlke, A.M. Haaparanta, V. Muhonen, K. Laine, Y. Bilotsky, M. Kellomaki, I. Kiviranta, The importance of controlled mismatch of biomechanical compliances of implantable scaffolds and native tissue for articular cartilage regeneration, Front. Bioeng. Biotechnol. 6 (2018) 187–197, doi:10.3389/fbioe.2018.00187.
[18] H. Petit-Eisenmann, E. Epailly, M. Velten, J. Radojevic, B. Eisenmann, H. Kremer, M. Kindo, Impact of prosthesis-patient mismatch on long-term functional capacity after mechanical aortic valve replacement, Can. J. Cardiol. 32 (2016) 1493–1499, doi:10.1016/j.cjca.2016.02.076.
[19] H. Tian, Z. Tang, X. Zhuang, X. Chen, X. Jing, Biodegradable synthetic polymers: preparation, functionalization and biomedical application, Prog. Polym. Sci. 37 (2012) 237–280, doi:10.1016/j.progpolymsci.2011.06.004.
[20] H. Ye, K. Zhang, D. Kai, Z. Li, X.J. Loh, Polyester elastomers for soft tissue engineering, Chem. Soc. Rev. 47 (2018) 4545–4580, doi:10.1039/c8cs00161h.
[21] Q. Chen, S. Liang, G.A. Thouas, Elastomeric biomaterials for tissue engineering, Prog. Polym. Sci. 38 (2013) 584–671, doi:10.1016/j.progpolymsci.2012.05.003.
[22] K.E. Washington, R.N. Kularatne, V. Karmegam, M.C. Biewer, M.C. Stefan, Recent advances in aliphatic polyesters for drug delivery applications, Wiley Interdiscip. Rev. Nanomed. Nanobiotechnol. 9 (2017) e1146–e1161, doi:10.1002/wnan.1446.
[23] H.R. Ihre, O.L.P. De Jesús, F.C. Szoka, J.M.J. Fréchet, Polyester dendritic systems for drug delivery applications: design, synthesis, and characterization, Bioconjug. Chem. 13 (2002) 443–452, doi:10.1021/bc010102u.
[24] I. Manavitehrani, A. Fathi, H. Badr, S. Daly, A. Negahi Shirazi, F. Dehghani, Biomedical applications of biodegradable polyesters, Polymers 8 (2016) 20–52 (Basel), doi:10.3390/polym8010020.
[25] T.K. Dash, V.B. Konkimalla, Poly-ϵ-caprolactone based formulations for drug delivery and tissue engineering: a review, J. Control. Release 158 (2012) 15–33, doi:10.1016/j.jconrel.2011.09.064.
[26] F.A.M.M. Gonçalves, A.C. Fonseca, M. Domingos, A. Gloria, A.C. Serra, J.F.J. Coelho, The potential of unsaturated polyesters in biomedicine and tissue engineering: synthesis, structure-properties relationships and additive manufacturing, Prog. Polym. Sci. 68 (2017) 1–34, doi:10.1016/j.progpolymsci.2016.12.008.
[27] S. Tajbakhsh, F. Hajiali, A comprehensive study on the fabrication and properties of biocomposites of poly(lactic acid)/ceramics for bone tissue engineering, Mater. Sci. Eng. C Mater. Biol. Appl. 70 (2017) 897–912, doi:10.1016/j.msec.2016.09.008.
[28] N. Goonoo, R. Jeetah, A. Bhaw-Luximon, D. Jhurry, Polydioxanone-based biomaterials for tissue engineering and drug/gene delivery applications, Eur. J. Pharm. Biopharm. 97 (2015) 371–391, doi:10.1016/j.ejpb.2015.05.024.
[29] K. Fukushima, Poly(trimethylene carbonate)-based polymers engineered for biodegradable functional biomaterials, Biomater. Sci. 4 (2016) 9–24, doi:10.1039/C5BM00123D.
[30] S. Ribeiro, A.M. Carvalho, E.M. Fernandes, M.E. Gomes, R.L. Reis, Y. Bayon, D.I. Zeugolis, Development and characterisation of cytocompatible polyester substrates with tunable mechanical properties and degradation rate, Acta Biomater. 121 (2021) 303–315, doi:10.1016/j.actbio.2020.11.026.
[31] P. Wu, D. Aroush, A. Asnacios, W. Chen, M. Dokukin, B. Doss, P. Durand-Smet, A. Ekpenyong, J. Guck, N. Guz, P. Janmey, J. Lee, N. Moore, A. Ott, Y. Poh, R. Ros, M. Sander, I. Sokolov, J. Staunton, N. Wang, G. Whyte, D. Wirtz, A comparison of methods to assess cell mechanical properties, Nat. Methods 15 (2018) 491–498, doi:10.1038/s41592-018-0015-1.
[32] D. Cigognini, D. Gaspar, P. Kumar, A. Satyam, S. Alagesan, C. Sanz-Nogues, M. Griffin, T. O'Brien, A. Pandit, D.I. Zeugolis, Macromolecular crowding meets oxygen tension in human mesenchymal stem cell culture - a step closer to physiologically relevant *in vitro* organogenesis, Sci. Rep. 6 (2016) 30746–30756, doi:10.1038/srep30746.
[33] J. Vandesompele, K. De Preter, F. Pattyn, B. Poppe, N. Van Roy, A. De Paepe, F. Speleman, Accurate normalization of real-time quantitative RT-PCR data by geometric averaging of multiple internal control genes, Genome Biol. 3 (2002) research0034.0031-research0034.0011, doi:10.1186/gb-2002-3-7-research0034.
[34] I. Barbosa, S. Garcia, V. Barbier-Chassefière, J.-.P. Caruelle, I. Martelly, D. Papy-García, Improved and simple micro assay for sulfated glycosaminoglycans quantification in biological extracts and its use in skin and muscle tissue studies, Glycobiology 13 (2003) 647–653, doi:10.1093/glycob/cwg082.
[35] S.R. Herlofsen, A.M. Kuchler, J.E. Melvik, J.E. Brinchmann, Chondrogenic differentiation of human bone marrow-derived mesenchymal stem cells in self-gelling alginate discs reveals novel chondrogenic signature gene clusters, Tissue Eng. Part A 17 (2011) 1003–1013, doi:10.1089/ten.TEA.2010.0499.
[36] S. Nemir, J. West, Synthetic materials in the study of cell response to substrate rigidity, Ann. Biomed. Eng. 38 (2010) 2–20.
[37] H. Lv, L. Li, M. Sun, Y. Zhang, L. Chen, Y. Rong, Y. Li, Mechanism of regulation of stem cell differentiation by matrix stiffness, Stem Cell Res. Ther. 6 (2015) 103.
[38] C. Loebel, R. Mauck, J. Burdick, Local nascent protein deposition and remodelling guide mesenchymal stromal cell mechanosensing and fate in three-dimensional hydrogels, Nat. Mater. 18 (2019) 883–891, doi:10.1038/s41563-019-0307-6.
[39] A.S. Chahal, M. Schweikle, C.A. Heyward, H. Tiainen, Attachment and spatial organisation of human mesenchymal stem cells on poly(ethylene glycol) hydrogels, J. Mech. Behav. Biomed. Mater. 84 (2018) 46–53, doi:10.1016/j.jmbbm.2018.04.025.
[40] Y.R. Shih, K.F. Tseng, H.Y. Lai, C.H. Lin, O.K. Lee, Matrix stiffness regulation of integrin-mediated mechanotransduction during osteogenic differentiation of human mesenchymal stem cells, J. Bone Miner. Res. 26 (2011) 730–738, doi:10.1002/jbmr.278.
[41] F.N. Kenny, Z. Drymoussi, R. Delaine-Smith, A.P. Kao, A.C. Laly, M.M. Knight, M.P. Philpott, J.T. Connelly, Tissue stiffening promotes keratinocyte proliferation through activation of epidermal growth factor signaling, J. Cell Sci. 131 (2018) jcs215780-jcs215795, doi:10.1242/jcs.215780.
[42] D.-.H. Kim, D. Wirtz, Predicting how cells spread and migrate: focal adhesion size does matter, Cell Adhes. Migr. 7 (2013) 293–296, doi:10.4161/cam.24804.
[43] M. Bao, J. Xie, N. Katoele, X. Hu, B. Wang, A. Piruska, W.T.S. Huck, Cellular volume and matrix stiffness direct stem cell behavior in a 3D microniche, ACS Appl. Mater. Interfaces 11 (2019) 1754–1759, doi:10.1021/acsami.8b19396.
[44] C. Yang, F.W. DelRio, H. Ma, A.R. Killaars, L.P. Basta, K.A. Kyburz, K.S. Anseth, Spatially patterned matrix elasticity directs stem cell fate, Proc. Natl. Acad. Sci. U. S. A. 113 (2016) E4439–E4445, doi:10.1073/pnas.1609731113.
[45] A. Elosegui-Artola, R. Oria, Y. Chen, A. Kosmalska, C. Perez-Gonzalez, N. Castro, C. Zhu, X. Trepat, P. Roca-Cusachs, Mechanical regulation of a molecular clutch defines force transmission and transduction in response to matrix rigidity, Nat. Cell Biol. 18 (2016) 540–548, doi:10.1038/ncb3336.
[46] M. Inui, G. Martello, S. Piccolo, MicroRNA control of signal transduction, Nat. Rev. Mol. Cell Biol. 11 (2010) 252–263, doi:10.1038/nrm2868.
[47] J.D. Mih, A. Marinkovic, F. Liu, A.S. Sharif, D.J. Tschumperlin, Matrix stiffness reverses the effect of actomyosin tension on cell proliferation, J. Cell Sci. 125 (2012) 5974–5983, doi:10.1242/jcs.108886.
[48] A. Skardal, D. Mack, A. Atala, S. Soker, Substrate elasticity controls cell proliferation, surface marker expression and motile phenotype in amniotic fluid-derived stem cells, J. Mech. Behav. Biomed. Mater. 17 (2013) 307–316, doi:10.1016/j.jmbbm.2012.10.001.
[49] A. Srinivasan, S.Y. Chang, S. Zhang, W.S. Toh, Y.C. Toh, Substrate stiffness modulates the multipotency of human neural crest derived ectomesenchymal stem cells via CD44 mediated PDGFR signaling, Biomaterials 167 (2018) 153–167, doi:10.1016/j.biomaterials.2018.03.022.
[50] M. Maleki, F. Ghanbarvand, M.Reza Behvarz, M. Ejtemaei, E. Ghadirkhomi, Comparison of mesenchymal stem cell markers in multiple human adult stem cells, Int. J. Stem Cells 7 (2014) 118–126, doi:10.15283/ijsc.2014.7.2.118.
[51] J. Xie, M. Bao, X. Hu, W.J.H. Koopman, W.T.S. Huck, Energy expenditure during cell spreading influences the cellular response to matrix stiffness, Biomaterials 267 (2021) 120494–120504, doi:10.1016/j.biomaterials.2020.120494.
[52] S. Masterton, M. Ahearne, Influence of polydimethylsiloxane substrate stiffness on corneal epithelial cells, R. Soc. Open Sci. 6 (2019) 191796–191809, doi:10.1098/rsos.191796.
[53] C. Shen, C. Yang, S. Xu, H. Zhao, Comparison of osteogenic differentiation capacity in mesenchymal stem cells derived from human amniotic membrane (AM), umbilical cord (UC), chorionic membrane (CM), and decidua (DC), Cell Biosci. 9 (2019) 17–27, doi:10.1186/s13578-019-0281-3.
[54] N. Liu, M. Zhou, Q. Zhang, T. Zhang, T. Tian, Q. Ma, C. Xue, S. Lin, X. Cai, Stiffness regulates the proliferation and osteogenic/odontogenic differentiation of human dental pulp stem cells via the WNT signalling pathway, Cell Prolif. 51 (2018) e12435–e12444, doi:10.1111/cpr.12435.
[55] J. Xu, W. Wang, M. Ludeman, K. Cheng, T. Hayami, J.C. Lotz, S. Kapila, Chondrogenic differentiation of human mesenchymal stem cells in three-dimensional alginate gels, Tissue Eng. Part A 14 (2008) 667–680, doi:10.1089/tea.2007.0272.
[56] S. Portron, V. Hivernaud, C. Merceron, J. Lesoeur, M. Masson, O. Gauthier, C. Vinatier, L. Beck, J. Guicheux, Inverse regulation of early and late chondrogenic differentiation by oxygen tension provides cues for stem cell-based cartilage tissue engineering, Cell. Physiol. Biochem. 35 (2015) 841–857, doi:10.1159/000369742.
[57] R. Rakic, B. Bourdon, M. Demoor, S. Maddens, N. Saulnier, P. Galéra, Differences in the intrinsic chondrogenic potential of equine umbilical cord matrix and cord blood mesenchymal stromal/stem cells for cartilage regeneration, Sci. Rep. 8 (2018) 1–16, doi:10.1038/s41598-018-28164-9.
[58] M.A. Szychlinska, G. Calabrese, S. Ravalli, N.L. Parrinello, S. Forte, P. Castrogiovanni, E. Pricoco, R. Imbesi, S. Castorina, R. Leonardi, M. Di Rosa, G. Musumeci, Cycloastragenol as an exogenous enhancer of chondrogenic differentiation of human adipose-derived mesenchymal stem cells. A morphological study, Cells 9 (2020) 347–363, doi:10.3390/cells9020347.
[59] A.L. Gale, R.L. Linardi, G. McClung, R.M. Mammone, K.F. Ortved, Comparison of the chondrogenic differentiation potential of equine synovial membrane-derived and bone marrow-derived mesenchymal stem cells, Front. Vet. Sci. 6 (2019) 178–187, doi:10.3389/fvets.2019.00178.
[60] M. Desancé, R. Contentin, L. Bertoni, T. Gomez-Leduc, T. Branly, S. Jacquet, J.-.M. Betsch, A. Batho, F. Legendre, F. Audigié, P. Galéra, M. Demoor, Chondrogenic differentiation of defined equine mesenchymal dtem cells derived from umbilical cord blood for use in cartilage repair therapy, Int. J. Mol. Sci. 19 (2018) 537–569, doi:10.3390/ijms19020537.
[61] S. Nürnberger, C. Schneider, G. van Osch, C. Keibl, B. Rieder, X. Monforte, A. Teuschl, S. Mühleder, W. Holnthoner, B. Schädl, Repopulation of an auricular cartilage scaffold, AuriScaff, perforated with an enzyme combination, Acta Biomater. 86 (2019) 207–222, doi:10.1016/j.actbio.2018.12.035.

[62] K. Pelttari, A. Winter, E. Steck, K. Goetzke, T. Hennig, B.G. Ochs, T. Aigner, W. Richter, Premature induction of hypertrophy during *in vitro* chondrogenesis of human mesenchymal stem cells correlates with calcification and vascular invasion after ectopic transplantation in SCID mice, Arthritis Rheum. 54 (2006) 3254–3266, doi:10.1002/art.22136.

[63] K. Sakimura, T. Matsumoto, C. Miyamoto, M. Osaki, H. Shindo, Effects of insulin-like growth factor I on transforming growth factor β1 induced chondrogenesis of synovium-derived mesenchymal stem cells cultured in a polyglycolic acid scaffold, Cells Tissues Organs 183 (2006) 55–61, doi:10.1159/000095509.

[64] T. Jiang, W. Liu, X. Lv, H. Sun, L. Zhang, Y. Liu, W.J. Zhang, Y. Cao, G. Zhou, Potent *in vitro* chondrogenesis of CD105 enriched human adipose-derived stem cells, Biomaterials 31 (2010) 3564–3571, doi:10.1016/j.biomaterials.2010.01.050.

[65] K. Liu, G.D. Zhou, W. Liu, W.J. Zhang, L. Cui, X. Liu, T.Y. Liu, Y. Cao, The dependence of *in vivo* stable ectopic chondrogenesis by human mesenchymal stem cells on chondrogenic differentiation *in vitro*, Biomaterials 29 (2008) 2183–2192, doi:10.1016/j.biomaterials.2008.01.021.

[66] E. Salonius, L. Kontturi, A. Laitinen, A. Haaparanta, M. Korhonen, J. Nystedt, I. Kiviranta, V. Muhonen, Chondrogenic differentiation of human bone marrow-derived mesenchymal stromal cells in a three-dimensional environment, J. Cell. Physiol. 235 (2020) 3497–3507, doi:10.1002/jcp.29238.

[67] A. Arora, A. Kothari, D.S. Katti, Pericellular plasma clot negates the influence of scaffold stiffness on chondrogenic differentiation, Acta Biomater. 46 (2016) 68–78, doi:10.1016/j.actbio.2016.09.038.

[68] D.A. Young, Y.S. Choi, A.J. Engler, K.L. Christman, Stimulation of adipogenesis of adult adipose-derived stem cells using substrates that mimic the stiffness of adipose tissue, Biomaterials 34 (2013) 8581–8588, doi:10.1016/j.biomaterials.2013.07.103.

[69] P.M. Gilbert, K.L. Havenstrite, K.E.G. Magnusson, A. Sacco, N.A. Leonardi, P. Kraft, N.K. Nguyen, S. Thrun, M.P. Lutolf, H.M. Blau, Substrate elasticity regulates skeletal muscle stem cell self-renewal in culture, Science 329 (2010) 1078–1081, doi:10.1126/science.1191035.

[70] N. Bouchonville, M. Meyer, C. Gaude, E. Gay, D. Ratel, A. Nicolas, AFM mapping of the elastic properties of brain tissue reveals kPa/μm gradients of rigidity, Soft Matter 12 (2016) 6232–6239, doi:10.1039/C6SM00582A.

[71] C. Then, J. Menger, G. Benderoth, M. Alizadeh, T.J. Vogl, G. Silber, A method for a mechanical characterisation of human gluteal tissue, Technol. Health Care 15 (2007) 385–398. 10.3233/THC-2007-15601

[72] L. Penuela, C. Negro, M. Massa, E. Repaci, E. Cozzani, A. Parodi, S. Scaglione, R. Quarto, R. Raiteri, Atomic force microscopy for biomechanical and structural analysis of human dermis: a complementary tool for medical diagnosis and therapy monitoring, Exp. Dermatol. 27 (2018) 150–155, doi:10.1111/exd.13468.

[73] P.F. Lozano, M. Scholze, C. Babian, H. Scheidt, F. Vielmuth, J. Waschke, B. Ondruschka, N. Hammer, Water-content related alterations in macro and micro scale tendon biomechanics, Sci. Rep. 9 (2019) 7887, doi:10.1038/s41598-019-44306-z.

[74] M. Kwacz, Z. Rymuza, M. Michalowski, J. Wysocki, Elastic properties of the annular ligament of the human stapes-AFM measurement, J. Assoc. Res. Otolaryngol. 16 (2015) 433–446, doi:10.1007/s10162-015-0525-9.

[75] M. Stolz, R. Raiteri, A.U. Daniels, M. VanLandingham, W.Baschong R., U. Aebi, Dynamic elastic modulus of porcine articular cartilage determined at two different levels of tissue organization by indentation-type atomic force microscopy, Biophys. J. 86 (2004) 3269–3283, doi:10.1016/S0006-3495(04)74375-1.

[76] S. Hengsberger, A. Kulik, P. Zysset, A combined atomic force microscopy and nanoindentation technique to investigate the elastic properties of bone structural units, Eur. Cell Mater. 1 (2001) 12–17, doi:10.22203/ecm.v001a02.